Interner Bericht
DESY S1-73/4
August 1973

A Pulsed Magnetic Lens for Positron Focusing
Numerical Calculation and First Measurements with a Prototype

by

G. Stange

Introduction

The positron focusing systems used in linear accelerators until now are rather involved because of the need for very high magnetic fields. If these fields are generated with D.C. current there is necessary quite a large volume for the coils and a very effective water cooling system.
This causes small reliability, which is especially bad because the positron convertor and its surrounding become severely radioactive.
The present positron convertor solenoid in the DESY LINAC II generates a field of about 18 kGauss at 500 A and has a power consumption of nearly 60 kW. Because of the complicated construction of the vacuum system and the attached coil system it is impossible to repair it in case of failure, when - additionally - it is radioactive.
Therefore the demand arose for a simple small system.

This paper describes a pulsed magnetic lens of the most simple construction. In the first part the lens data are evaluated theoretically by numerical methods. The following parts describe the technical realization of a prototype system and first measurement data. They show that the efficiency of the pulsed lens is at least the same as with the present DC - 18 kGauss - solenoid, although the prototype system was not the optimal one from theoretical calculations.

1. The Short Magnetic Lens

The short magnetic lens to be analyzed in this paper is a small helicoidal coil without iron. It has rotational symmetry and is therefore of the most simple construction. The data of the optimal coil are developed in the following section. There are several technical limits to be kept in mind in order to get a practically possible solution. These are:

a) The pulse current may not be higher than 5500 A, because it is to be switched with a hydrogen thyratron. The max. current for commercially available thyratrons is 6000 A.

b) Since the pulse generation is performed by capacitor discharge one has to optimize the inductance of the coil and capacitance as to give reasonable pulse length and not too high voltage requirements.

As a result the optimization procedure is a rather complex process, involving purely physical arguments and technical limitations. (Lit.KR 68, PA 67)

1.1 The Magnetic Lens as Part of the Beam Transport System for Positrons in the Linac. General Requirements

The goal is to replace the present 18 kGauss-DC-solenoid by the pulsed lens. As the lens acts together with a complex positron transport system we give a short description of LINAC II in the positron operation mode. (For further information lit. FE 72).
LINAC II is able to accelerate both electrons and positrons up to energies of about 500 MeV and 400 MeV respectively. It has 12 accelerator sections, each of about 5m length. Behind the fifth section the positron convertor is located (Fig.1). The positrons emerging from the target are focused by an 18 kGauss - solenoid into the input of the next accelerator section 6. On this section and the following, number 7, a 4 kGauss - solenoid takes care of further focusing and keeps the beam small in diameter. When leaving section 7 the beam emittance is small enough as to be handled in a periodic FODO-channel on sections 8 to 12 (lit.WI. 68). The FODO-channel consists of alternating focusing and defocusing quadrupoles with a drift space in between. The optical matching between the 4 kGauss - solenoid and the FODO - channel is obtained by a quadrupole dublett between these two sections.
Now, the pulsed magnetic lens we are dealing with, should have focusing properties fitting to the remaining system.

1.2 Numerical Calculation of the Focusing Properties

As was just pointed out, the numerical calculation of optimal lens data has to take into account the optical properties of the following transport system, especially of the solenoidal field in section 6, thereby keeping in mind the above mentioned technical restrictions. Furthermore the geometrial arrangement between target and the input flange of section 6 gives rise to additional limitations in the optical acceptance. (Fig.2)
Therefore the theoretical procedure is:

a) calculation of lens field
b) calculation of 4 kGaus fringe field
c) acceptance calculation of section 6 entrance
d) trajectory calculation for positrons with
   decision whether accepted or not.

1.2.1 Field Calculation for the Lens

The expressions for the axial and radial field components of a short lens are elliptic integrals. The solution is not analytically expressible. In cyclindrical coordinates we get (lit. PA. 67):

$$H_{rp} = \frac{\mathcal{J}}{4\pi} \int_R \int_z \int_\varphi \frac{R \cos\varphi \,(z-z_p)}{\left[R^2 - 2Rr_p\cos\varphi + r_p^2 + (z-z_p)^2\right]^{3/2}} \, dR\,dz\,d\varphi \qquad (1.2.1)$$

$$H_{zp} = \frac{\mathcal{J}}{4\pi} \int_R \int_z \int_\varphi \frac{R^2 - Rr_p\cos\varphi}{\left[R^2 - 2Rr_p\cos\varphi + r_p^2 + (z-z_p)^2\right]^{3/2}} \, dR\,dz\,d\varphi \qquad (1.2.2)$$

$\mathcal{J}$ ... current density
R, φ, z ... coordinates of the coil
r_p, Z_p ... coordinates of the point in which the field is to be calculated
H_{rp}, H_{zp} ... magnetic field at point (r_p, z_p)

These integrals are deduced from BIOT - SAVART'S LAW. For H_{rp} two integrations may be carried out analytically, over z and R, for H_{zp} one only, over z, because the other one over R leads to too complex expressions (although it is possible in principle).
The integration yields:

$$H_{rp} = \frac{\mathcal{J}}{4\pi}\left[\int_0^{2\pi} \cos\varphi \left(\sqrt{(R-r_p\cos\varphi)^2 + r_p^2\sin^2\varphi + (z-z_p)^2} + r_p\cos\varphi \cdot \operatorname{arsinh}\frac{R - r_p\cos\varphi}{\sqrt{r_p^2\sin^2\varphi + (z-z_p)^2}}\right) d\varphi\right]_{R_1}^{R_2}{}_{-\frac{l}{2}}^{+\frac{l}{2}} \qquad (1.2.3)$$

$$H_{zp} = \frac{\mathcal{J}}{4\pi} \int_R \int_0^{2\pi} \frac{(R^2 - Rr_p\cos\varphi)(z-z_p)}{(R^2 - 2Rr_p\cos\varphi + r_p^2)\sqrt{R^2 - 2Rr_p\cos\varphi + r_p^2 + (z-z_p)^2}} \, dR\,d\varphi \Big|_{-l/2}^{+l/2} \qquad (1.2.4)$$

These integrals have been solved numerically with a program called 'lens'. The integration technique follows SIMPSON'S RULE (lit. DA. 67, ZU. 65). In Figs.3-6 we have plotted numerical values of axial and radial field for two different lens geometries. It follows that a coil with only two layers of windings has a much more homogenous field over the lens aperture than a coil with 4 layers.
As it turns out later (1.2.4) from the calculation of positron trajectories a homogenous field is more useful for our purpose.

1.2.2 Fringe Field Calculation for the 4kGaus-Solenoid on Accelerator Section 6:

The positrons have to pass about 150mm fringe field between the positron lens and the beginning of focus 6 solenoid. Therefore the fringe field plays an important role in the overall focusing efficiency.
The magnetic field of a long solenoid ($l \gg d$), which has homogenous density of windings over the whole length has half the maximum field strength at its ends. In order to compensate this there have been mounted special flat coils to each of the ends of the long solenoids.

The principal expressions for calculating the fringe field are those from section 1.2.1. In our case, however, some simplifications are allowed. Since we deal with near axis trajectories compared to the coil dimensions, so-called paraxial rays, we suppose

$$r_p \ll R \quad .$$

Then the integral (1.2.2) for H_{zp} may be solved analytically. This leads to the expression:

$$H_{zp} = \frac{J}{4\pi}\left[-R\,\mathrm{arsinh}\frac{z-z_p}{R} + (z-z_p)\,\mathrm{arsinh}\frac{R}{z-z_p} - R\cdot\ln\frac{R}{z-z_p+\sqrt{(z-z_p)^2+R_a^2}}\right]_{R_i}^{R_a}\Bigg|_{z_1}^{z_2} \qquad (1.2.5)$$

From this we derive the radial field component for near axis points using Maxwell's equation:

$$\mathrm{div}\ B = \mu \cdot \mathrm{div}\ H \quad = 0$$

and with rotational symmetry

$$\frac{1}{r_p}\,\frac{\partial}{\partial r_p}\,(r_p \cdot H_{rp}) + \frac{\partial H_{zp}}{\partial z_p} = 0$$

$$\frac{\partial}{\partial r_p}\,(r_p \cdot H_{rp}) = - r_p\,\frac{\partial H_{zp}}{\partial z_p}$$

Since for small $r_p << 1$

$$\frac{\partial H_{zp}}{\partial Z_p} \neq f(r_p)$$

we get

$$H_{rp} = - \frac{1}{2} r_p \quad \frac{\partial H_{zp}}{\partial z_p} \qquad (1.2.6)$$

with H_{zp} from (1.2.5).

With these formulae the fringe field has been calculated by a computer program called 'fringe-field'. It takes into account the influence of the flat compensating coils mentioned above. Not included is the effect of an iron shield surrounding the whole coil system. But since there are no end plates and the diameter of the iron tube is rather large the influence of the iron should be within 10% as can be shown by comparison between field measurement and calculation.

A plot of the computed fringe field is shown in Fig.7.

1.2.3 Acceptance of Section 6:

When the positrons have passed the positron lens and the fringe field, the question arises which of them are accepted in the narrow accelerating structure of section 6.

The initial conditions of the particle when entering section 6 have to be in such limits that the spiral which the particle will run through never exceeds the aperture.

In Fig.8 the principal relationships are shown. The maximum possible spiral radius of the particle ρ, obeys

$$(\rho \sin\phi + r_o)^2 + \rho^2 \cos^2\phi = (R - \rho)^2 \qquad (1.2.7)$$

which leads to

$$\rho = \frac{R^2 - r_o^2}{2(R+r_o \sin\phi)} \qquad (1.2.8)$$

ρ may be expressed by the transverse momentum, p_{tr} . With (1.2.8) one gets:

$$p_{tr}(R + r_o \sin\phi) = \frac{eB(R^2 - r_o^2)}{2} \qquad (1.2.9)$$

Additionally

$$p_{tr} = r_o' p_o \sqrt{1 + \frac{r_o^2}{r_o'^2} \phi_o'^2} \qquad (1.2.10)$$

p_o ... total momentum
r_o, r_o' ... initial conditions, differentiation
ϕ_o' with respect to s in direction of positron path

Combining (1.2.9) and (1.2.10) one may resolve for r_o' :

$$r_o' = \pm \frac{1}{R\, p_o} \left[\left(\frac{eB(R^2-r_o^2)}{2} - r_o\, p_\theta \right)^2 - R^2 p_\theta^2 \right] \qquad (1.2.11)$$

with $p_\theta = r_o \cdot p_o \cdot \phi_o'$.

For given field in section 6, B, and given initial conditions r_o, ϕ_o' , (1.2.11) supplies the maximum possible r_o' in order to accept the particle. Therefore this formula may be used to decide, whether a particle, when having passed from the target to section 6, is accepted or not. (lit.WI. 66).

1.2.4 Numerical Calculation of Positron Trajectories Through the Lens and the Fringe Field of Section 6

The motion of a charged particle (charge e) in a magnetic field of rotational symmetry obeys the following system of 3 second order differential equations:

$$Z'' = -\frac{e}{mc} r \cdot \phi' \cdot B_r$$

$$r'' = \frac{e}{mc} r\phi' \cdot B_z + r \cdot \phi'^2 \qquad (1.2.12)$$

$$\phi'' = \left[\frac{e}{mc} (rz'B_r - rr'B_z) - 2rr'\phi' \right] \frac{1}{r^2}$$

where " ' " means differentiation with respect to s, the path length of the particle. In (1.2.12) it has been made use of the relation

$$\frac{d}{dt} = \frac{d}{ds} \cdot \frac{ds}{dt} = c \cdot \frac{d}{ds}$$

for relativistic particles.
This system may not be solved analytically. A computer program following the procedure of RUNGE - KUTTA has been combined with the programs 'lens' and 'fringe - field' mentioned above. In each point arrived at by the Runge - Kutta procedure the total field from the lens and superimposed fringe field is calculated in order to perform the next Runge - Kutta step (lit. ZU. 65).

In addition it is possible to vary all kinds of initial conditions of the positrons, for the lens data as parameters. In each case the efficiency in terms of the accepted solid angle is computed.

With this program it has been tried to find an optimum solution for the positron lens within the given technical limits.

1.2.5 The Optimization Procedure and Discussion of the Results

Since the positron production as a function of the angle, the target depth and -material and electron beam power is quite well-known from measurement data and Monte-Carlo calculations the acceptance of a focusing system in terms of the solid angle is a characteristic value for estimating the expected positron current.
Looking for the optimal lens data, several sometimes contradictory requirements have to be met. The final result is a compromise between these requirements. These requirements are:

1. Accepted positron energy should be higher than 7 MeV, because the positron production is not known very well below. From measurements done at LINAC II it is about 20% less* than at 10 MeV (lit. LM. 71).
2. The accepted energy band should be as broad as possible.
3. Maximum accepted solid angle.
4. Lens current may not exceed 5500 A because of thyratron current capability.
5. The inductance of the coil may not be too high (in the order of some μH) because of pulse length and mainly voltage requirements.
6. The lens must be of simple construction, because the conductor has to be a directly water-cooled tube. No insulation material may be used, for the coil is located in a vacuum housing under heavy Gamma-radiation bombardment.

In Fig.9 several results are shown with the acceptance of the present 18 kGauss-DC-solenoid for comparison (lit. AM. 63). It turns out, that a coil with the following data is a reasonable compromise:

length	45 mm
inner diameter	25 mm
outer diam.	45 mm
number of turns	16
current	5 500 A

For this type of coil several further properties have been studied theoretically.

Fig.3 and 4 show the axial and radial field at I = 5 000 A at different distances from the axis. The axial field is homogenous within about 10% over the whole aperture. The radial field has peaks at the coil ends. The main difference in optical respect between the present 18 kGauss-DC-solenoid and this lens is the following: In the DC-solenoid the target is immerged into a homogenous axial field and the positrons see a radial field only at the exit from the lens. In our case the positrons see the fringe field on either side of the lens, which is causing stronger focusing. In this respect the pulsed lens is acting as a short lens more than the DC-solenoid.

Fig.10 shows the dependence of the accepted solid angle on the radial distance of the positron origin on the target. In 2.2 we will use this relationship for calculating the emittance.

* at 7 MeV

Fig.11 shows the influence of the distance target - coil on the focusing properties. A spacing of 5mm should give optimum results.
Finally Fig.12 and 13 explain the influence of distance target - solenoid 6 and field in solenoid 6 respectively.

2. Calculation of Positron Beam

2.1. Expected Intensity

In this section the expected positron current will be calculated for two different coil types:

Type 1: The optimum coil according to the description in 1.2.5.

Type 2: a coil with the following data

length	40 mm
inner diameter	25 mm
outer diameter	41 mm
number of turns	12
current	5000 A

The coil under 2. has been used as a prototype for first measurements. Its acceptance is shown in Fig. 9. From the calculations it is not the optimal one, but for technical reasons we had to choose it.

From measurements and Monte-Carlo calculations (Lit. HA 67) we know that the positron production is following the formulae:

$$\dot{n}(\theta) = \dot{n}_o \cdot e^{-\theta/\theta_o} \quad ; \quad \theta_o = 0.305 \text{ rad} \hat{=} 17.45^o \tag{2.1}$$

The positron yield per unit energy, unit angle and incident electron is

$$n_o = 2.4 \cdot 10^{-4} \; [E_{e^-} \text{ [MeV]} - 25] \; / \; (\text{MeV} \cdot \text{sterad} \cdot \text{incident } e^-) \tag{2.2}$$

n .... number of positrons
E_{e^-} .... energy of the incident electrons
θ .... angle between system axis and direction of positron

These formulae are valid for

$$55 \text{ MeV} \leq E_{e-} \leq 220 \text{ MeV}$$

$$0.5\ X_o \leq t \leq 3\ X_o$$

$$8 \text{ MeV} \leq E_{e^+} \leq 0.2\ E_{e-}$$

X_o .... radiation length
t .... target thickness
E_{e+} .... positron energy

These conditions are fulfilled in our case. We use a tungsten target of 1.5 X_o and electron energies of about 200 MeV.

The electron beam parameters we used in the experiment are:

$$E_{e-} = 200 \text{ MeV}$$
$$I_{e-} = 280 \text{ mA}$$

Now the total positron current becomes:

$$I_{e+} = \int_{\Omega} \int_{E} n(\Omega) \cdot I_{e-}\, d\Omega\, dE \qquad (2.3)$$

with $\Omega = \pi\theta^2$ for small angles θ.

lens type 1:

For this case the acceptance area $\Omega(E)$ is shown in Fig. 10 with the spot size of the positron source as parameter. It is decreasing with the radial distance of the positron origin from the system axis. Therefore we have to know the spot size of the positron source which is nearly identical with the spot size of the electron beam, because the shower doesn't spread very much within 1.5 radiation lengths. (Lit. HA 67).

From measurements at LINAC II we know that without special focusing of the electron beam - possible with a quadrupole dublett in front of the target - about 60 % beam transmission is attainable through a 3 mm circular hole at the target location.

Taking into account this effect we have to evaluate the integral (2.3) based on the acceptance curve for 3 mm spot size (Fig. 10).

The integration limits are taken so as to have $\pm$ 0.5 % $\Delta E/E$ with respect to the linac end energy of the positrons - 300 MeV - around the accepted middle energy of 10 MeV, i.e. 8.5 MeV to 11.5 MeV. Furthermore we suppose, that only 60 % of the total electron current are useful for our system. This estimation should not be too optimistic since we neglect 40 % at all of the total electron beam. For the total positron beam we then get:

$$I_{e+\ \text{total}} = 2.5\ \text{mA}$$

By path length differences between axial and off-axis positrons in the lens, Focus 6 and 7 and FODO-channel the positron bunches are broadened, which leads to a deterioration of the energy spectrum. These effects may be estimated theoretically (Lit. FE 72). We know from measurements that about 65 % of total current are within 1 % energy bin, for 10 MeV positrons

$$I_{e+}\ (1\ \%\ \Delta E/E) = 1.6\ \text{mA}.$$

lens type 2:

A similar calculation with the acceptance of Fig. 9 leads to

$$I_{e+\ \text{total}} = 1.84\ \text{mA}$$

$$I_{e+}\ (1\%\ \Delta E/E) = 1.2\ \text{mA}.$$

Here it was taken into account that the positron production at 7 MeV is about 20 % less than at 10 MeV middle energy of the acceptance region (Lit. LM 71).

Since lens type 2 has been used for first measurements with the same data of the electron beam we have a possibility to compare the theoretical results with the measurement. This will be done in Section 4 of this report.

2.2. Expected Emittance

Taking an effective spot size for the positron beam of 3 mm diameter as we did in 1.2. we are able to get a rough estimation of the emittance if we plot the max. accepted angle (Fig. 10) versus the radial distance inside the energy band 8.5 MeV - 11.5 MeV (Fig. 14). We get:

$$\varepsilon = 60\ \pi \text{ mrad} \cdot \text{cm}$$

The acceptance of a long 4 kGauss - solenoid with a circular aperture of 2 cm diameter has been shown by H. Wiedemann to be (Lit. WI 66):

$$\varepsilon = \frac{600}{E} \cdot \pi \text{ with E in MeV.}$$

For positrons of 10 MeV this is 60 π mrad cm. This may be seen as a confirmation of our calculation procedure, in which the acceptance of Section 6 was taken to decide whether a particle is useful or not. We conclude that we have utilized the full aperture of Section 6. The only ways of increasing the positron current are therefore:

1. Reduction of the positron emittance by focusing the electron beam
2. Increasing the total electron beam.

With an end energy of 360 MeV - which is a typical value in the moment with 12 accelerator sections - we have an emittance of:

$$\varepsilon = 1.67\ \pi \text{ mrad cm (at 360 MeV)}$$

3. Technical Realization

In a first prototype system we used a coil of type 2 (Section 2.). It had a solid conductor of rectangular cross section 2.5 × 5.0 mm. The target was of tungsten with 1.5 radiation lengths thickness, surrounded by a copper ring with water-cooling (Fig. 2). In front of the target an SEM-disk was located with a

circular hole in its middle. It acted as a monitoring device for checking proper steering of the electron beam. Ideally the SEM-signal should be zero if the beam passes through the hole.

Fig. 2 shows the schematic arrangement of SEM, target and coil as well as the beginning of solenoid 6. Photograph 15 shows the upper flange of the convertor-housing with the coil etc. and high voltage lead throughs.

An important construction detail of the coil is, that the connections are as close together as possible to keep the dipole field due to each separate connector small, which would cause unliked steering effects. Therefore we used a special winding technique.

Fig. 16 shows the complete vacuum system. By a remote control drive mechanism the whole system may be moved on system axis for the positron mode or completely retracted for the electron mode of operation.

The pulse current through the coil is generated by capacitor discharge. The principal circuit is shown in Fig. 17. The charging power supply is working with a resonance operation and De-Q'ing system for stabilization. The main thyratron, which is switching the discharge circuit is triggered synchronous with the linac repetition frequency. Normally this frequency is 50 Hz. But as we didn't use a water-cooled coil we had to drive the system with 50/16 Hz only.

The coil was connected to the thyratron by two flat copper conductors very close to each other to keep the wave impedance small.

The following part gives some theoretical aspects of the electrical circuit.

3.1. Coil-Inductance

For the lens type 2 (see Section 2) the inductance becomes (Lit. PH 63):

$$L = \mu_o \frac{N^2}{4\pi} \cdot D \cdot K(\lambda,\rho) \quad \text{with} \quad \lambda = \frac{L}{D}\ ,\ \rho = \frac{D_o - D_i}{2D} \qquad (3.1)$$

N	.....	number of turns
D	.....	average diameter
K	.....	correcting factor (see Lit. PH 63)
1	.....	coil length
$D_{o,i}$	.....	outer, inner diameter

In our case, with K = 4.8, we get:

$$L = 2.28\ \mu H$$

3.2. Capacitor

Since coil and capacitor form a resonant circuit, we have

$$\frac{T}{2} = \Pi \sqrt{L \cdot C} \qquad (3.2)$$

and

$$U = \sqrt{\frac{L}{C}} \cdot I \qquad (3.3)$$

where T is the period of the resonant circuit. By the thyratron operation we only get one half period of current for each firing cycle. Between two pulses the capacitor is charged up again. In order to have a flat top of the pulse within 5 % for at least 1 µsec we should have $T/2 \geq 5$ µsec. With a capacitor of 2 µF we get:

$$\frac{T}{2} = \Pi \sqrt{2.28 \cdot 2}\ \mu sec = 6.7\ \mu sec$$

and

$$U = \sqrt{2.28/2} \cdot 5500\ V = 6000\ V \text{ at } I_{coil} = 5500\ A$$

The capacitor has been designed especially for pulse operation with coaxial connections and low inductance.

In the real circuit, we used for the prototype system, we measured somewhat increased values. For a pulse current of 5000 A we had

$$u = 8000\ V \text{ at } T/2 = 8\ \mu sec.$$

This is due to an increased inductance of the coil plus connections.

4. Experimental Results and Comparison with Theory

First we give the experimental results for the case, for which we have calculated the current in Section 2:

$$I_{e_-} = 280 \text{ mA}$$

$$E_{e_-} = 200 \text{ MeV}$$

$$I_{lens} = 5000 \text{ A}$$

$$B_{6+7} = 4 \text{ kGauss}$$

	measurement	theory
$I_{e+total}$	2.18 mA	1.84 mA
$I_{e+}(1\%\Delta E/E)$	1.26 mA	1.2 mA

The influence of additional focusing of the electron beam may be seen from the following table

$$I_{e_-} = 210 \text{ mA}$$

$$E_{e_-} = 200 \text{ MeV}$$

positron current

	without focusing	with focusing
$I_{e+total}$	1.7	2.0 mA
$I_{e+}(1\%\Delta E/E)$	1.03	1.2 mA

Comparing measurement with theory we may state that the theoretical estimation has not been too optimistic, since the theoretical values are lower than the measured ones.

The effect of focusing is about 20 % which is in good agreement with theory (see Section 2).

An additional DC-coil in the fringe field region in order to compensate for the descending field of Section 6 brought about 10 % increase in total positron current. On the other hand such a coil has the big disadvantage that it is very difficult to be mounted in the narrow region between convertor housing and the input flange of Section 6. For maintenance reasons one should have a most simple mechanical system, which may be easily removed in case of failure. Whereever possible the system should allow the use of long tools because of the high radioactivity to be expected. Therefore we did all the other measurements without this additional coil.

The problem of proper aligning the coil with respect to the linac axis has only been studied qualitatively. In our test system we adjusted the coil by eyesight. We didn't use special devices to fix it inside the vacuum housing except by the two coil connections (conductors to and from the coil).

Bad aligning of the coil or steering components of the field should have an awful influence on the positron yield as may be seen from the following simple calculations:
The deflection angle at the lens exit of a trajectory which is on axis at the lens entrance is determined by the transverse field component, B_{tr}:

$$\psi_{exit} = \int_{\substack{\text{coil}\\\text{length}}} \frac{ds}{\rho} = \int \frac{B_{tr} \cdot e}{p}\, ds \qquad (4.1)$$

with ρ .... radius of curvature
B_{tr} .... transverse magnetic field
p .... particle momentum

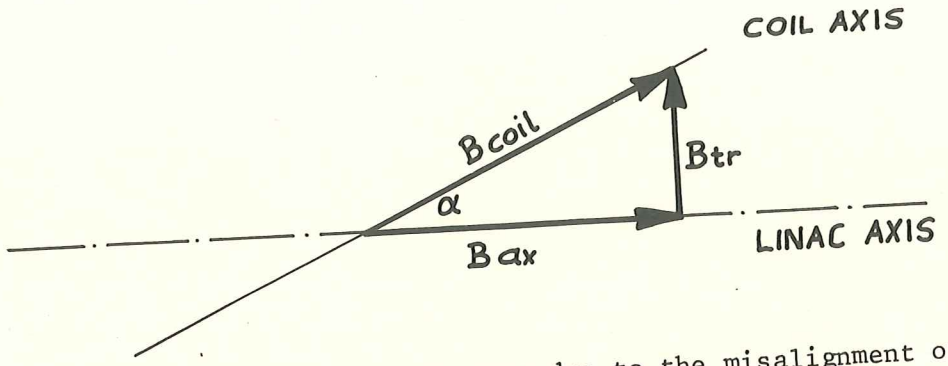

Fig. 18 Transverse steering field component due to the misalignment of the lens

From Figure 20 it follows:

$$B_{tr} = B_{coil} \cdot \sin \alpha \tag{4.2}$$

With $B_{coil} \approx 20$ kGauss and an effective coil length of 40 mm we get

$$\psi_{exit} = \frac{e}{p} \sin \alpha \cdot 20 \text{ k}\Gamma \cdot 4 \cdot 10^{-2} \text{ m}$$

and for a particle with p = 10 MeV/c

$$\psi_{exit} = 2.4 \sin \alpha$$

So, if we have a coil misalignment of 10^{o}, an on axis particle at the entrance would be deflected by 24^{o} at the exit.

A similar problem of severe influence is existing for a coil centered on the linac axis but an off-axis spot. In this case the whole positron beam is kicked off the system axis.

This has been confirmed by very sensitive electron beam steering in the experiment. As a consequence one has to take care of accurate adjusting devices for a final technical system.

With 8 μsec base length of the current pulse we got about 1.5 μsec flat top in the analyzed beam. As mentioned above this may be changed by properly choosing

the capacitance of the discharge circuit.
Summarizing the results, we got at least the same positron intensities as with the present DC-solenoid, although we didn't use an optimized test system. Taking lens type 1 (Section 2) there should be possible a further increase as theory shows.

5. Future Development

The prototype system we used is not able to run at 50 Hz repetition frequency. We have to build a directly water-cooled coil with a hollow conductor. As final solution we intend to take lens type 1. Furthermore we try to use a fixed target. In the moment we don't know, whether this is possible, because we didn't test it in the vacuum system at full beam power. Tests with a fixed target in air looked quite hopeful.
Since about 7 kW average beam power are turned into heat in the convertor and its neighbourhood we have to develop a proper vacuum housing and collimators with water-cooling to withstand this power.

Acknowledgement

I wish to thank Dr. A. Febel for many useful discussions and his interest in this project.
J. Scholz I want to thank for building the whole mechanical and electrical equipment and O. Schrader for the construction of the target.
Further thanks are due to the whole LINAC II crew for their assistance during the test of the prototype system.

Literature

AM 63 F. Amman, R. Andreani, LNF - 6346, Internal note No. 206, 1.7.63

DA 67 Ph. J. Davis, Ph. Rabinowitz, Numerical Integration, Blaisdell Publishing Comp. 1967

FE 72 A. Febel, G. Stange, Internal report DESY-S1-72/3, Aug. 1972

HA 67 J. Haissinski, Nucl. Instr. Meth. 51, p. 181-196, 1967

KR 68 D. J. Kroon, Laboratory magnets, Philips Technical Library, 1968

LM 71 LINAC-Messbuch, 13.11.70-13.7.1971

PA 67 D. H. Parkinson, B. E. Mulhall, The Generation of High Magnetic Fields, Heywood Books, London, 1967

PH 63 E. Philippow, Taschenuch Elektrotechnik, Bd. 1, VEB Verlag Technik, Berlin, 1963

SL 68 The Stanford Two-Mile Accelerator, 1968, W.A. Benjamin

WI 66 H. Wiedemann, DESY internal report H-14, Nov. 1966

WI 68 H. Wiedemann, DESY 68/5, Jan. 1968

ZU 65 R. Zurmühl, Praktische Mathematik, 5. Aufl., Springer Verlag Berlin, 1965.

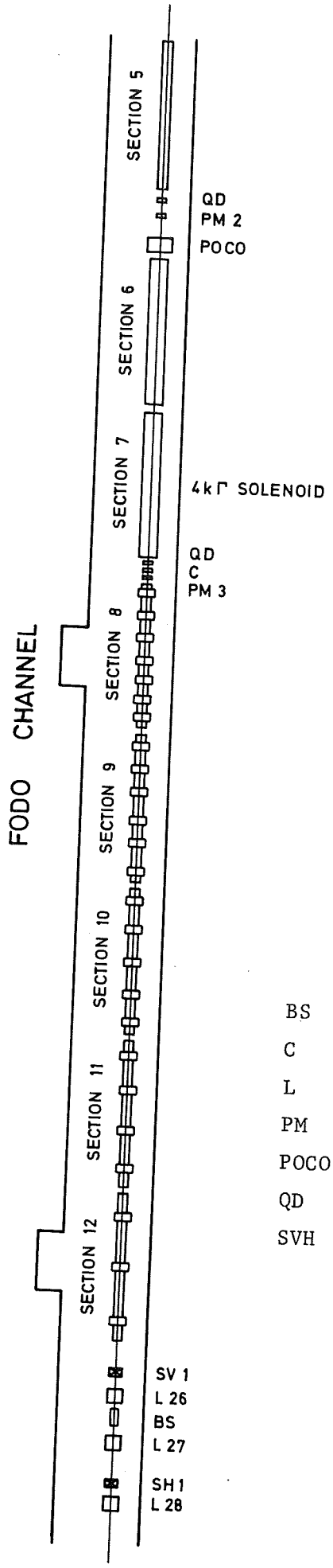

BS = BEAM SHUTTER

C = COLLIMATOR

L = LENS

PM = BEAM INTENSITY AND POSITION MONITOR

POCO = POSITRON CONVERTER

QD = QUADRUPOLE-DOUBLET

SVH = STEERING COIL VERTICAL, HORIZONTAL

FIG. 1

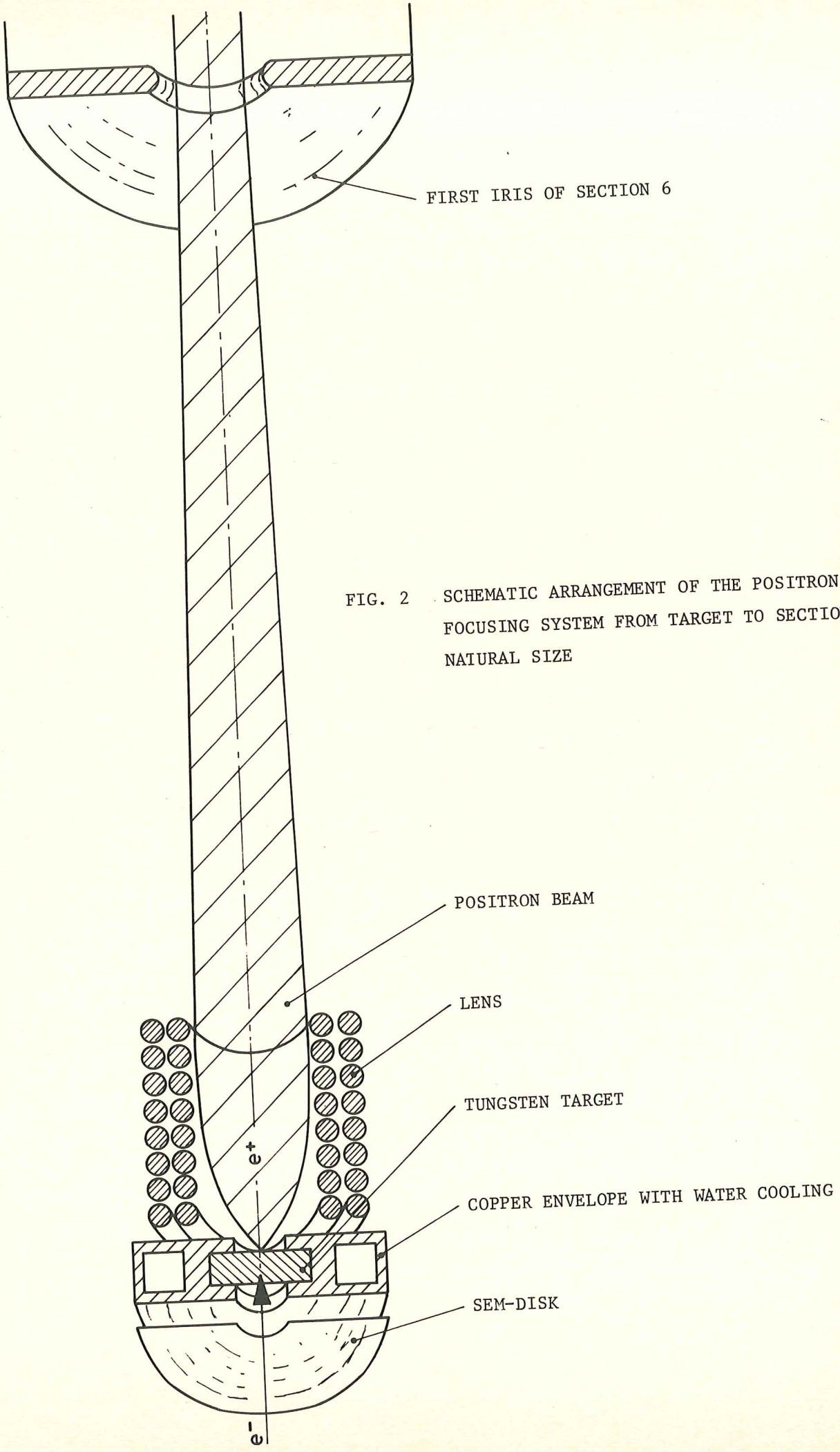

FIG. 2 SCHEMATIC ARRANGEMENT OF THE POSITRON FOCUSING SYSTEM FROM TARGET TO SECTION 6, NATURAL SIZE

FIG. 3 DISTRIBUTION OF AXIAL FIELD OF COIL WITH THE FOLLOWING DATA:

NUMBER OF TURNS	N = 16
LENGTH	L = 45MM
INNER DIAMETER	D_i = 25MM
OUTER DIAMETER	D_o = 45MM
OUTER DIAMETER OF CONDUCTOR	D_c = 4MM
CURRENT	I = 5000A

(see schematic drawing)

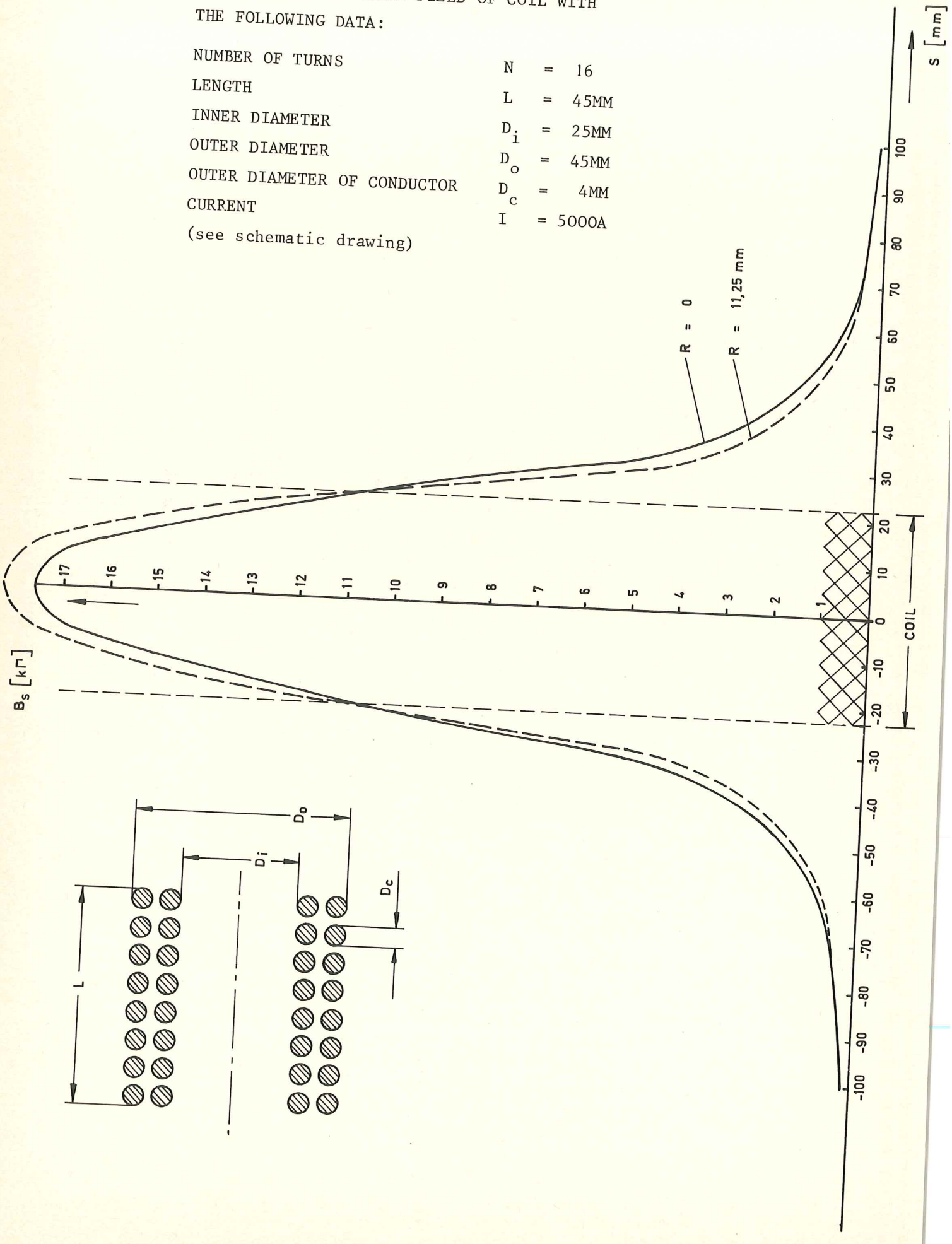

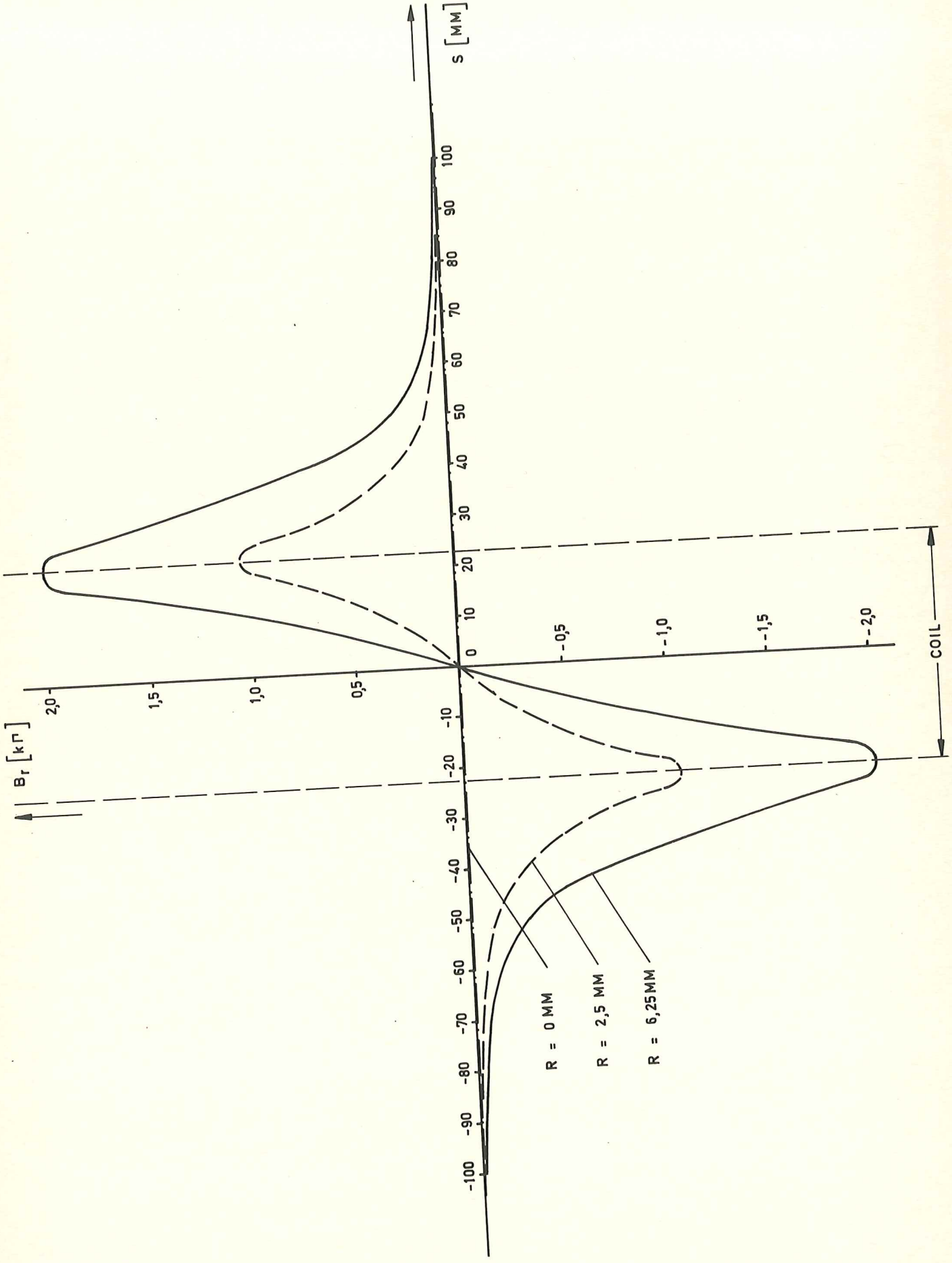

FIG. 4 DISTRIBUTION OF RADIAL MAGNETIC FIELD OF THE COIL, SPECIFIED IN FIG. 3

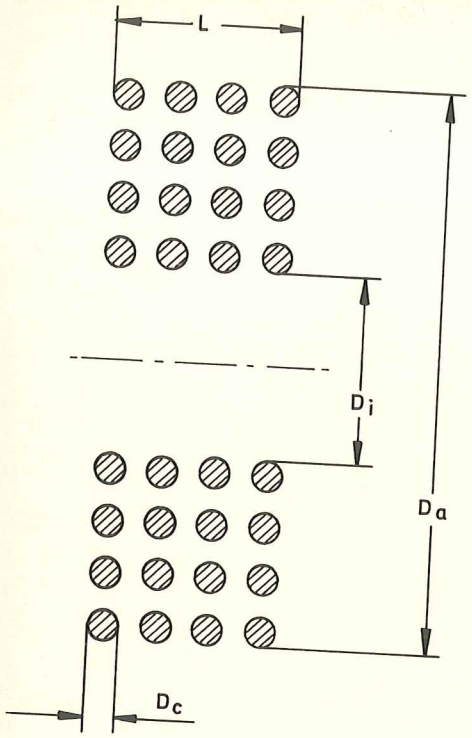

FIG. 5 DISTRIBUTION OF AXIAL FIELD OF A COIL WITH THE FOLLOWING DATA

NUMBER OF TURNS	N	=	16
LENGTH	L	=	25MM
INNER DIAMETER	D_i	=	25MM
OUTER DIAMETER	D_a	=	75MM
OUTER DIAMETER OF CONDUCTOR	D_c	=	4MM
CURRENT	I	=	5000A

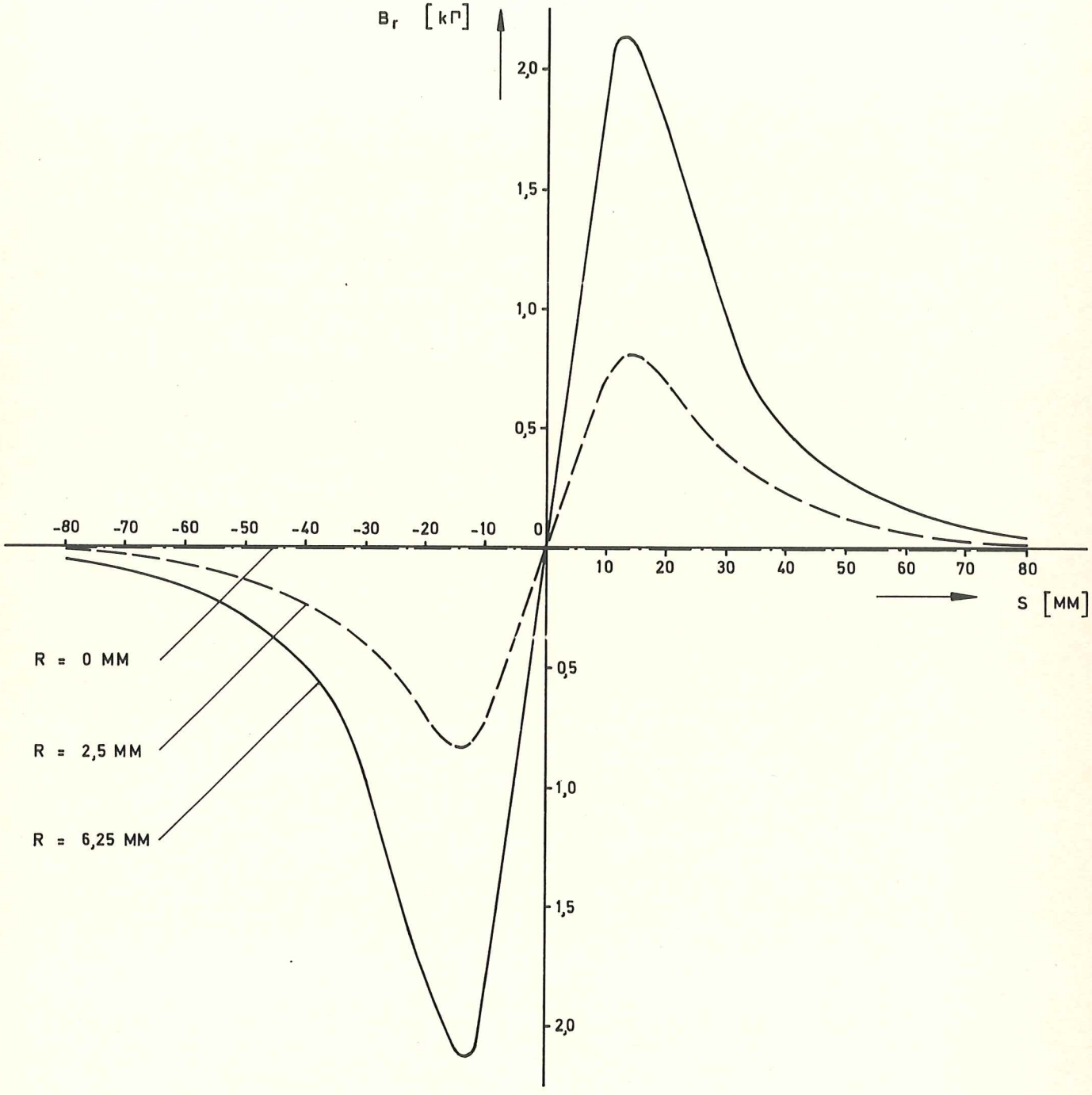

FIG. 6 DISTRIBUTION OF RADIAL MAGNETIC FIELD OF THE COIL, SPECIFIED IN FIG. 3

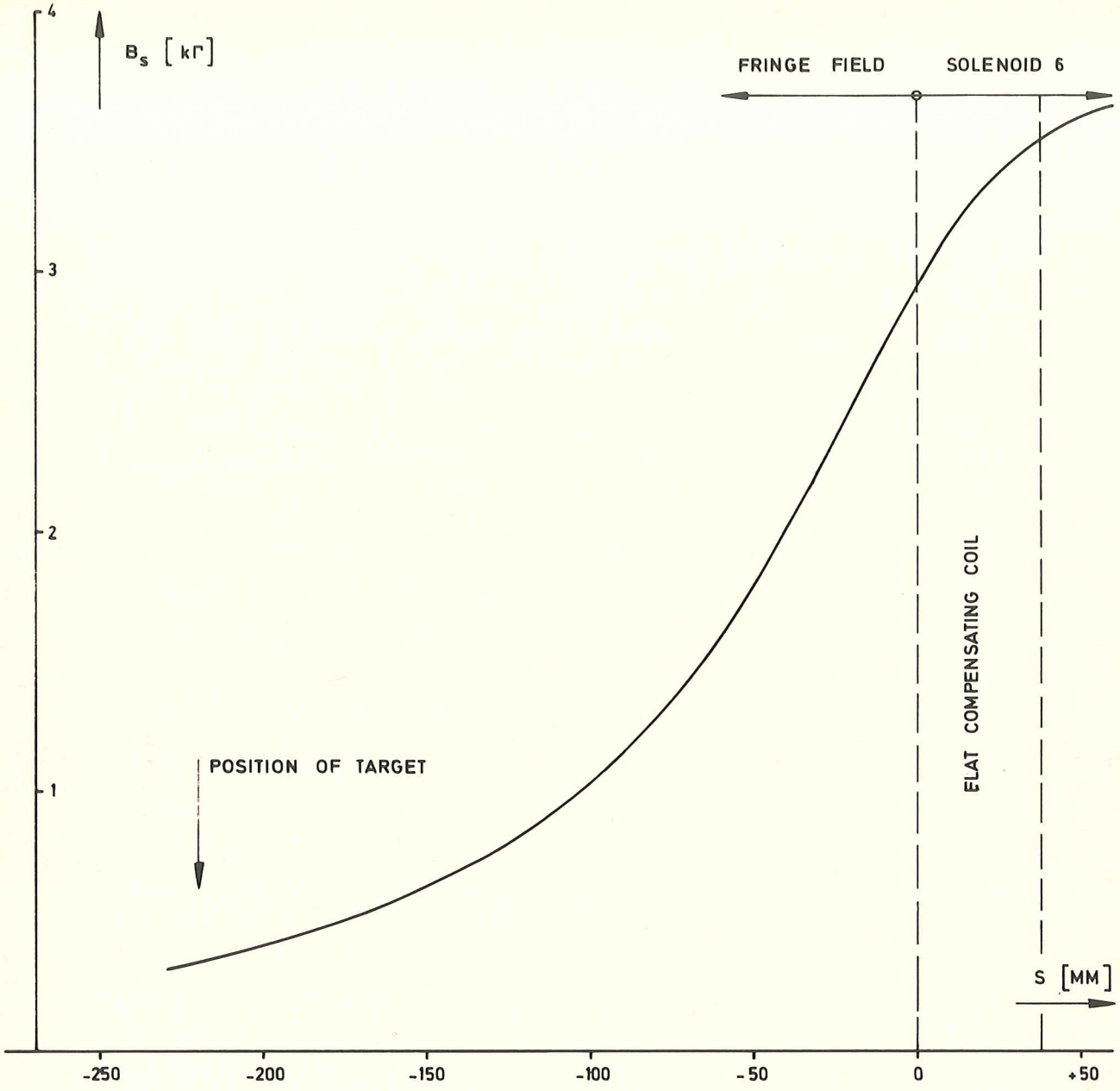

FIG. 7 FRINGE FIELD OF SOLENOID 6 (CALCULATED)

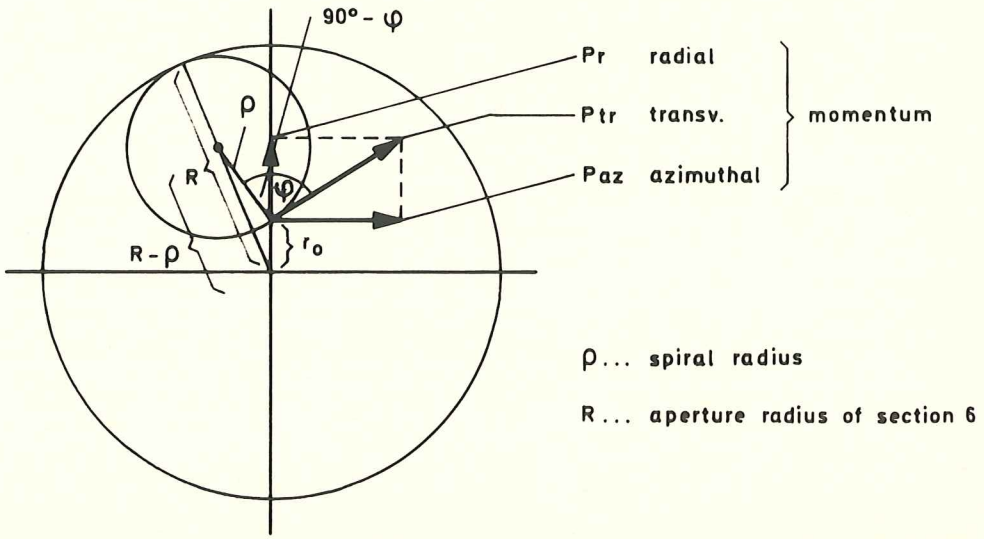

FIG. 8 ACCEPTANCE OF SECTION 6

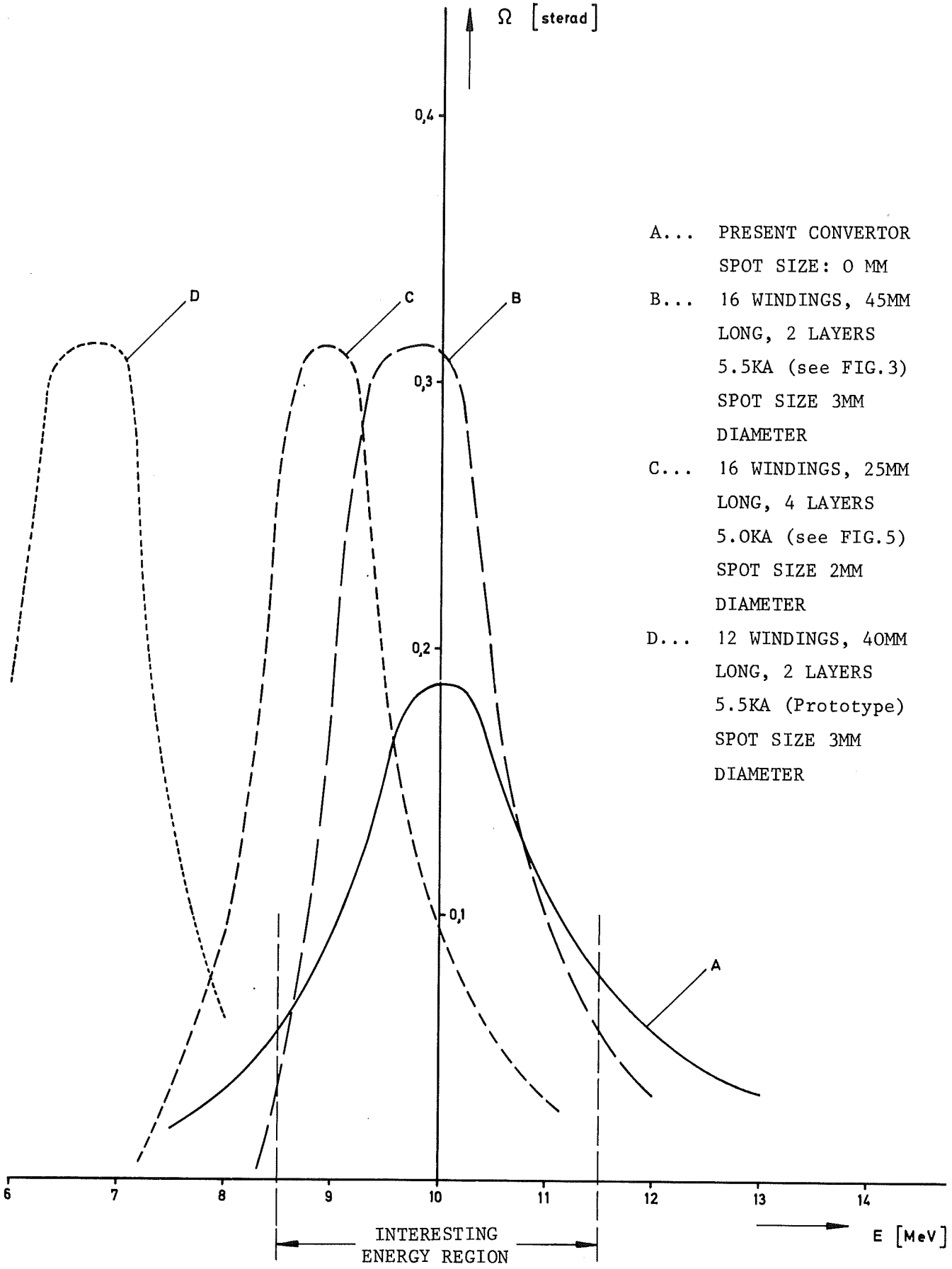

FIG. 9 ACCEPTANCE AREA OF DIFFERENT LENS GEOMETRIES

FIELD IN SECTION 6 : B = 4kGAUSS

DISTANCE TARGET-SECTION 6 : 220MM

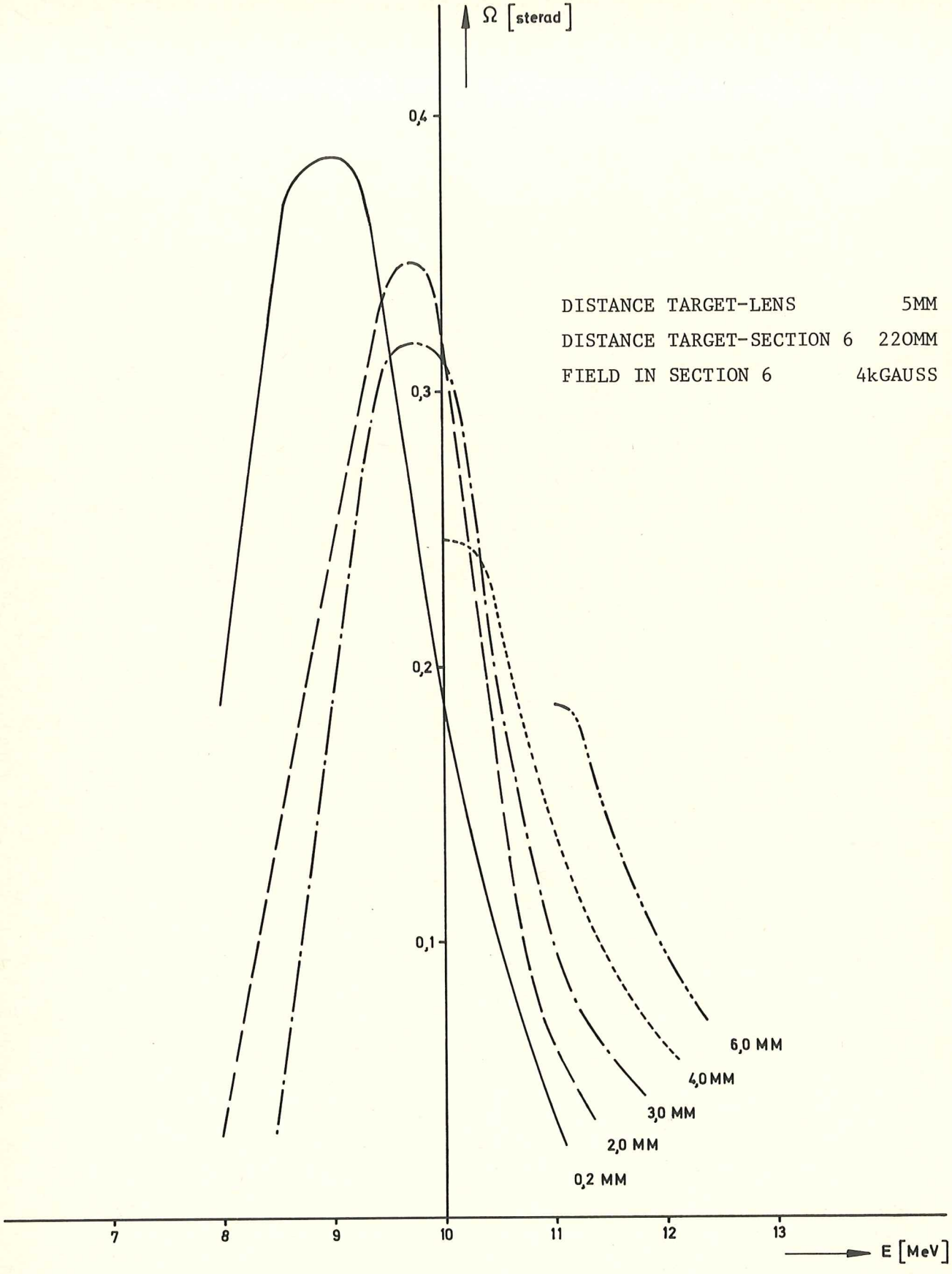

FIG. 10 THE ACCEPTANCE AREA WITH THE SPOT SIZE OF THE POSITRON SOURCE AS PARAMETER.
(FOR THE LENS ON FIG.3 WITH I = 5500A)

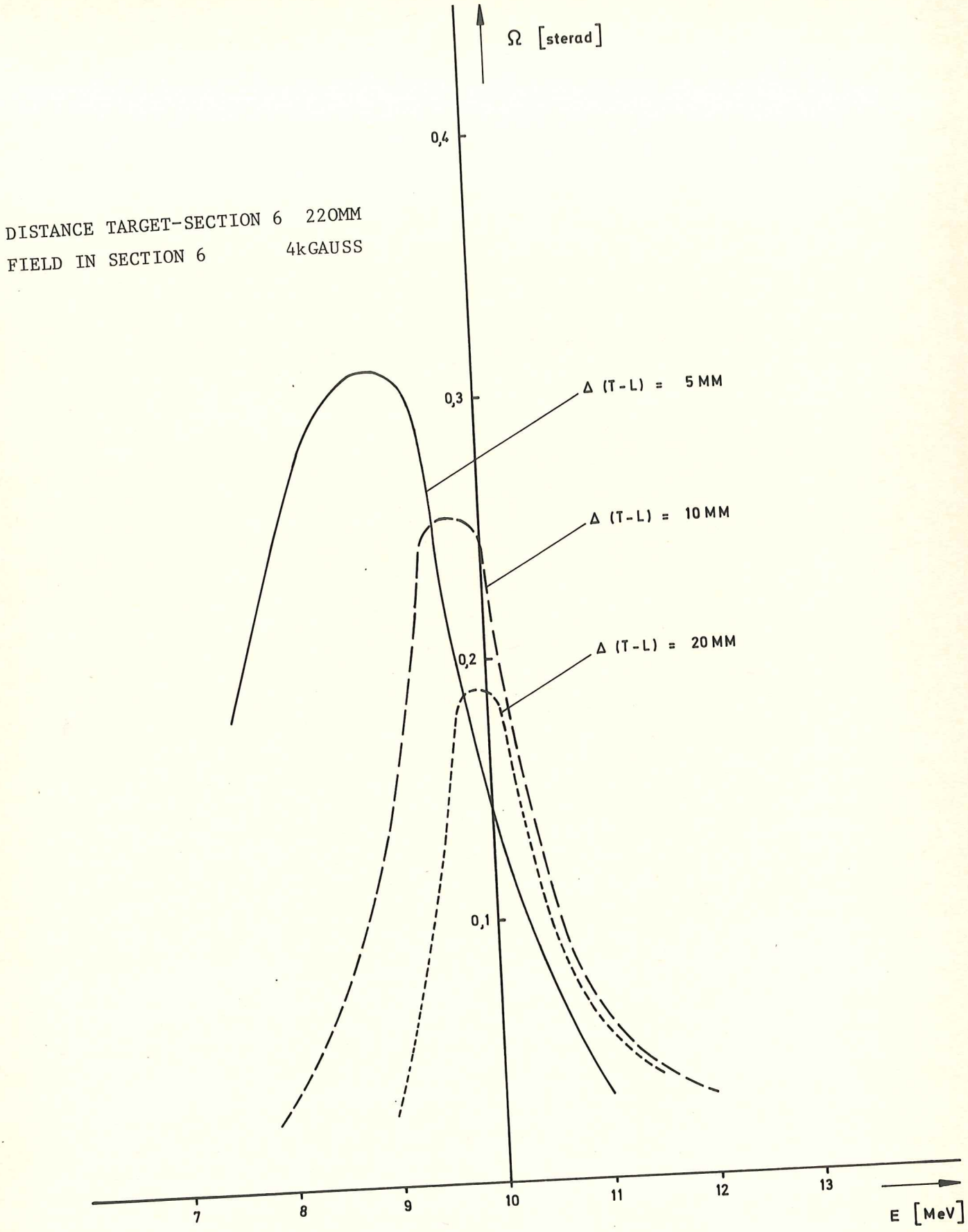

FIG. 11 THE ACCEPTANCE AREA WITH DISTANCE TARGET-COIL AS PARAMETER
(FOR THE LENS ON FIG.3 WITH I = 5000A)

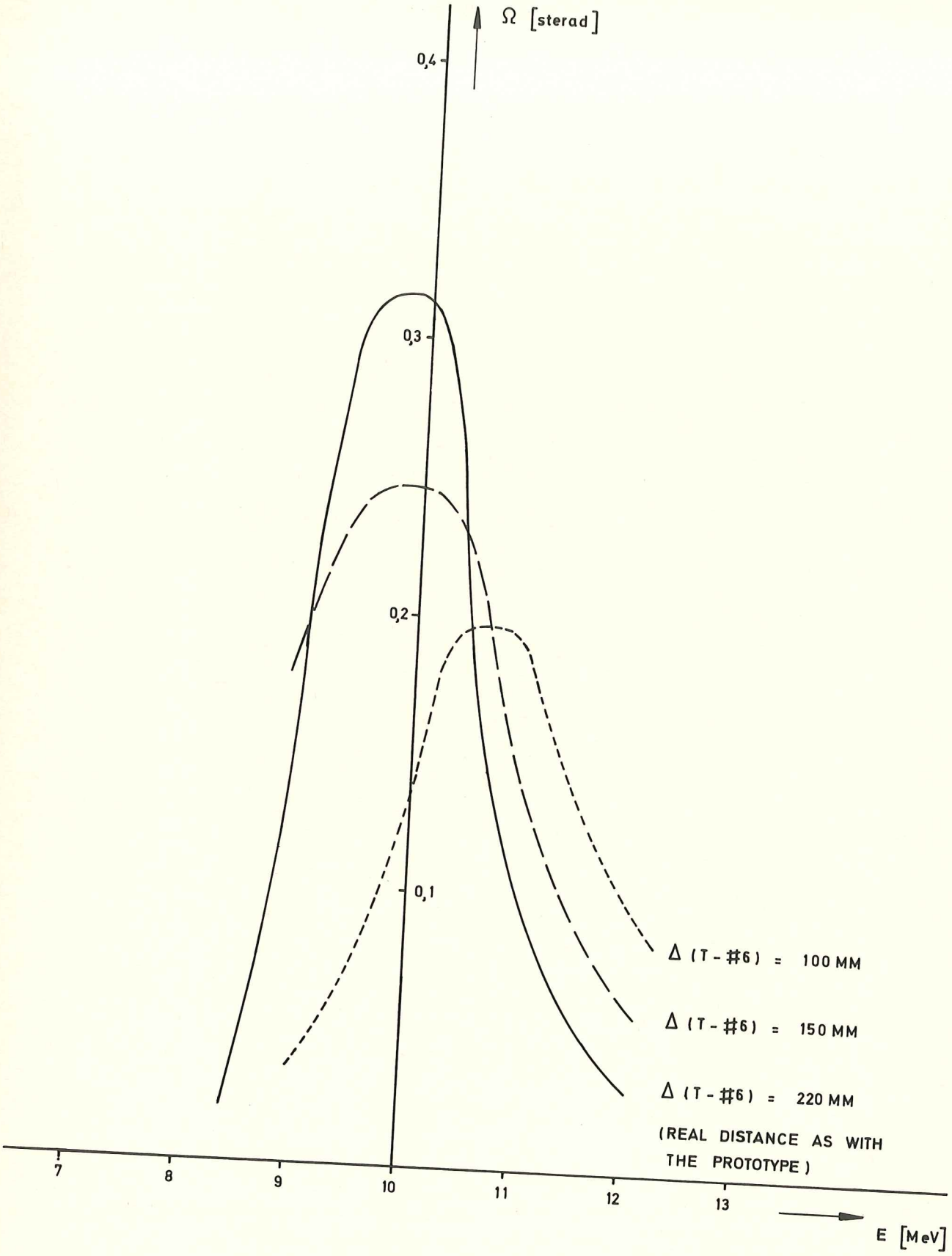

FIG. 12 ACCEPTANCE WITH DISTANCE TARGET-SOLENOID 6 AS PARAMETER (LENS OF FIG.3 WITH I = 5500A, DISTANCE TARGET-LENS 5 MM, SPOT SIZE 3 MM DIAMETER)

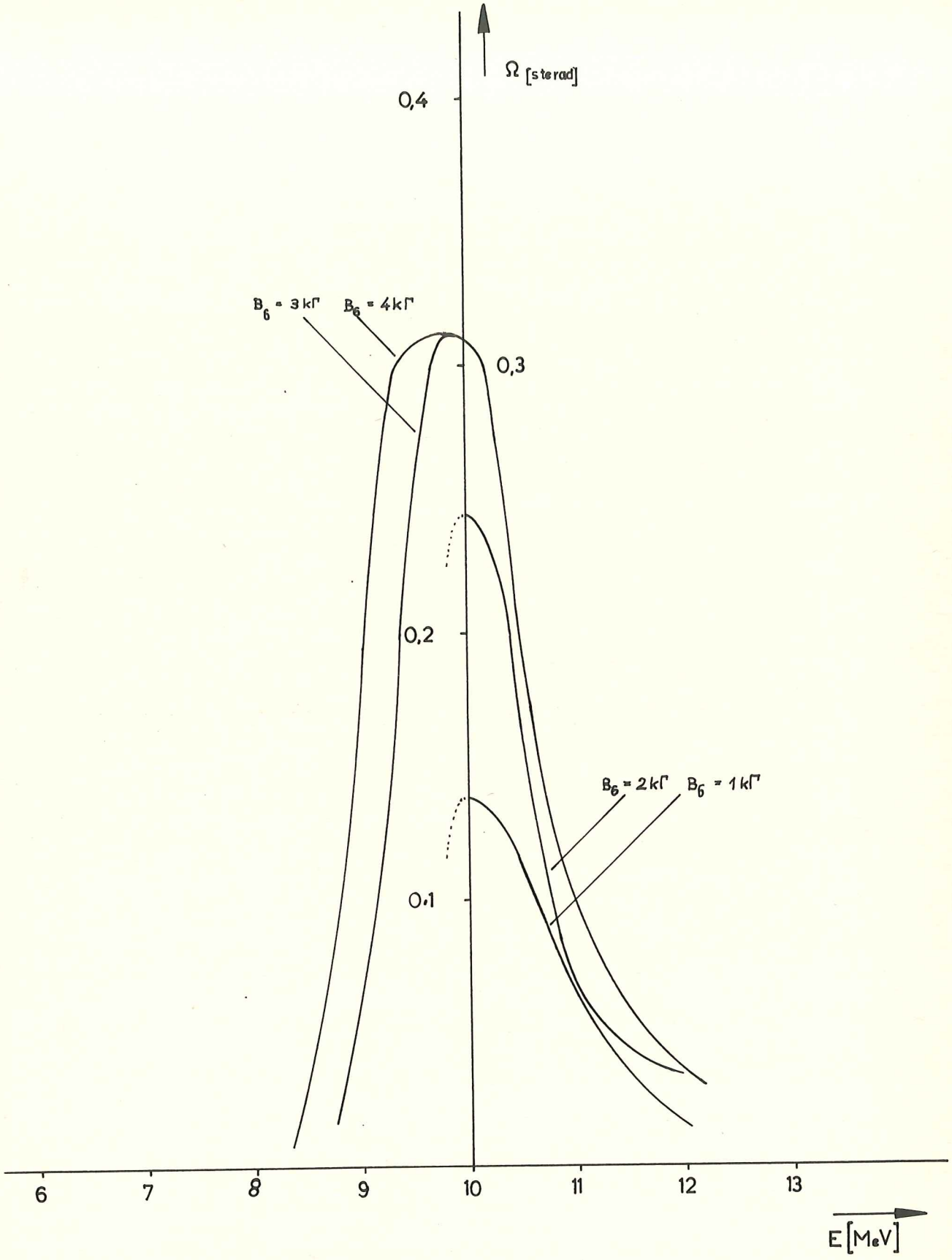

FIG. 13 ACCEPTANCE OF THE FOCUSING SYSTEM AS A FUNCTION OF THE SOLENOID FIELD IN SECTION 6 WITH LENS TYPE 1 AND THE FOLLOWING PARAMETERS:

DISTANCE TARGET-LENS	5 MM
DISTANCE TARGET-SECTION 6	220 MM
BEAM SPOT SIZE	3 MM
LENS CURRENT	5500 A

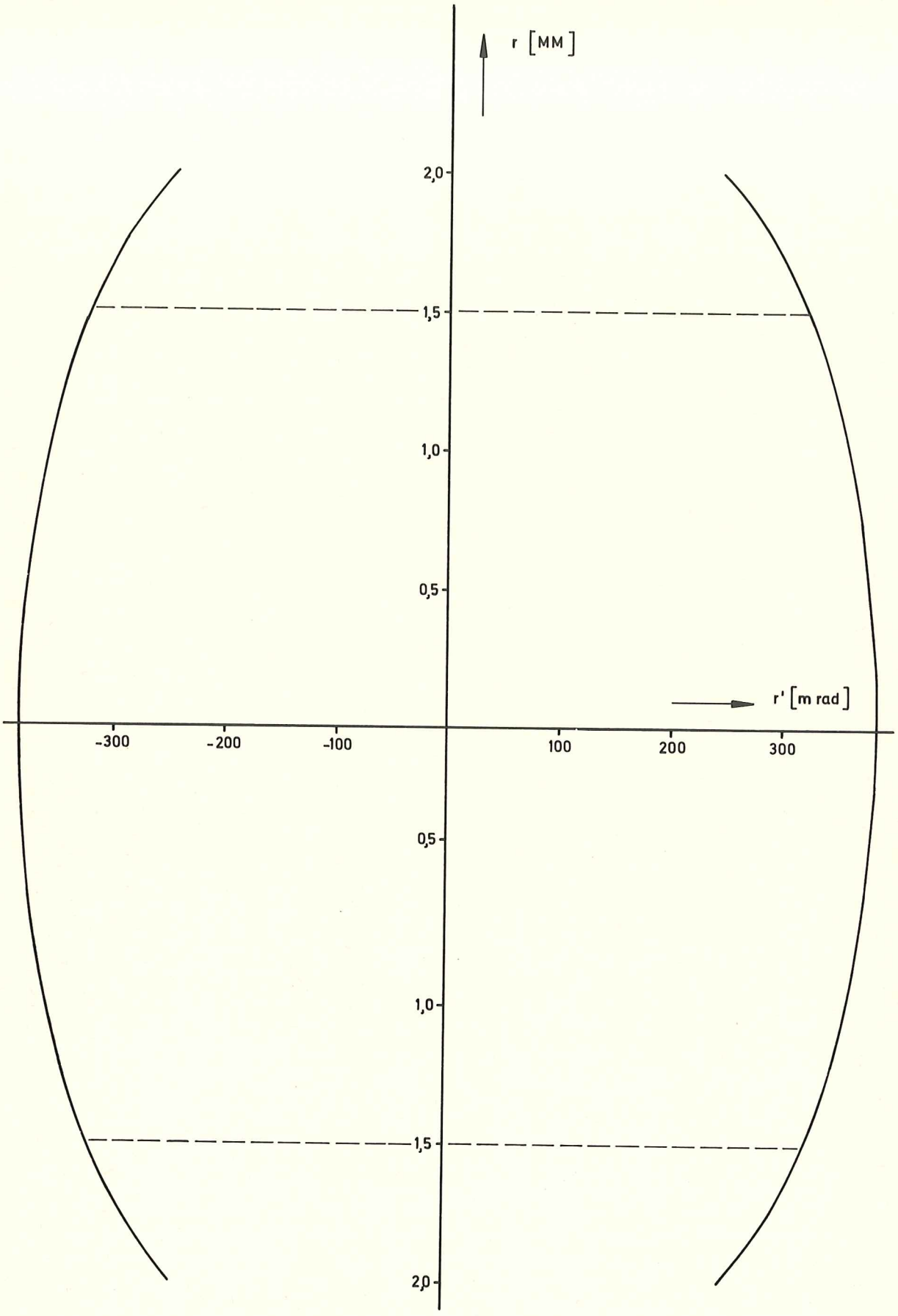

FIG. 14 ACCEPTANCE OF THE SYSTEM LENS-SOLENOID 6 (FIG.2)
WITH I_{LENS} = 5500A, B_6 = 4kGAUSS AND A SPOT SIZE
OF 3 MM DIAMETER (FROM FIG.10)
ENERGIE RANGE : 8,5 - 11,5 MeV

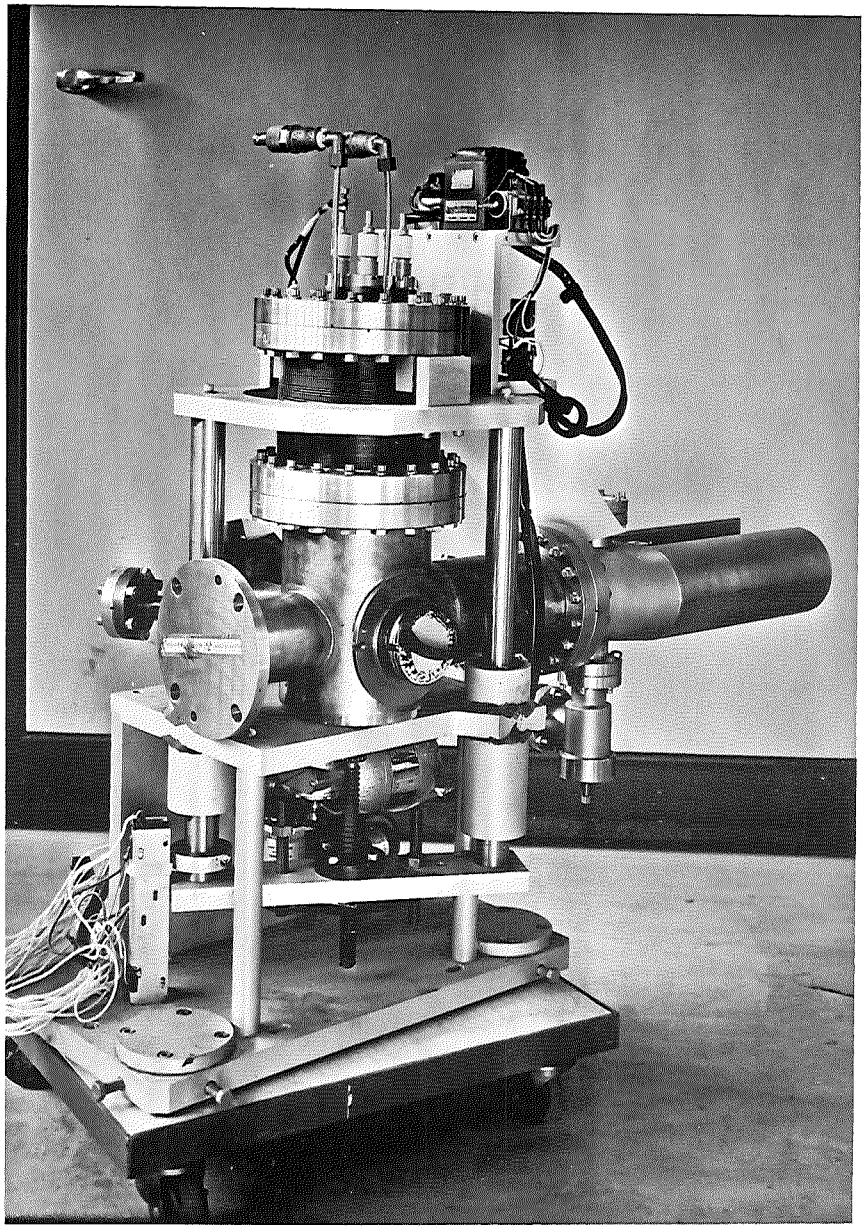

FIG. 16 THE CONVERTOR HOUSING

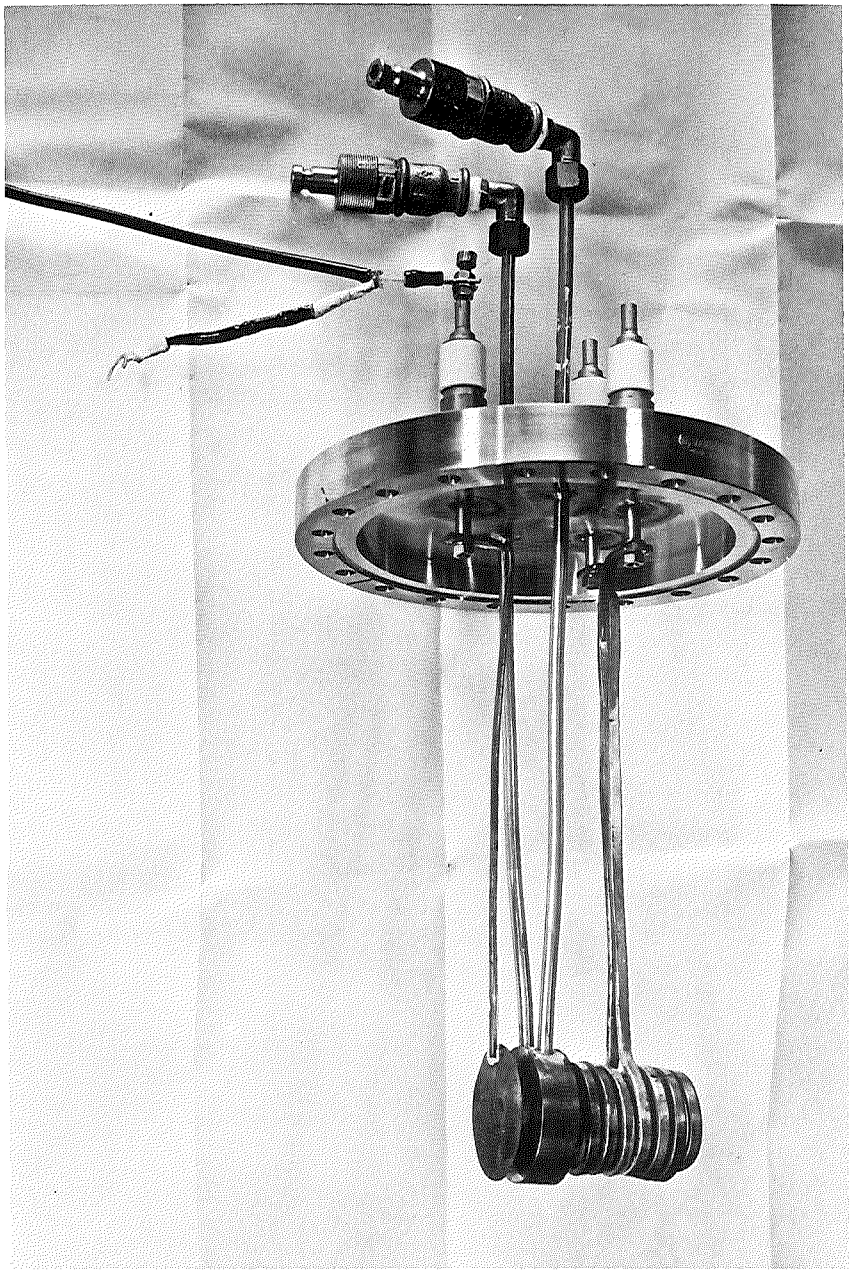

FIG. 15 THE CONVERTOR INSIDE THE VACUUM

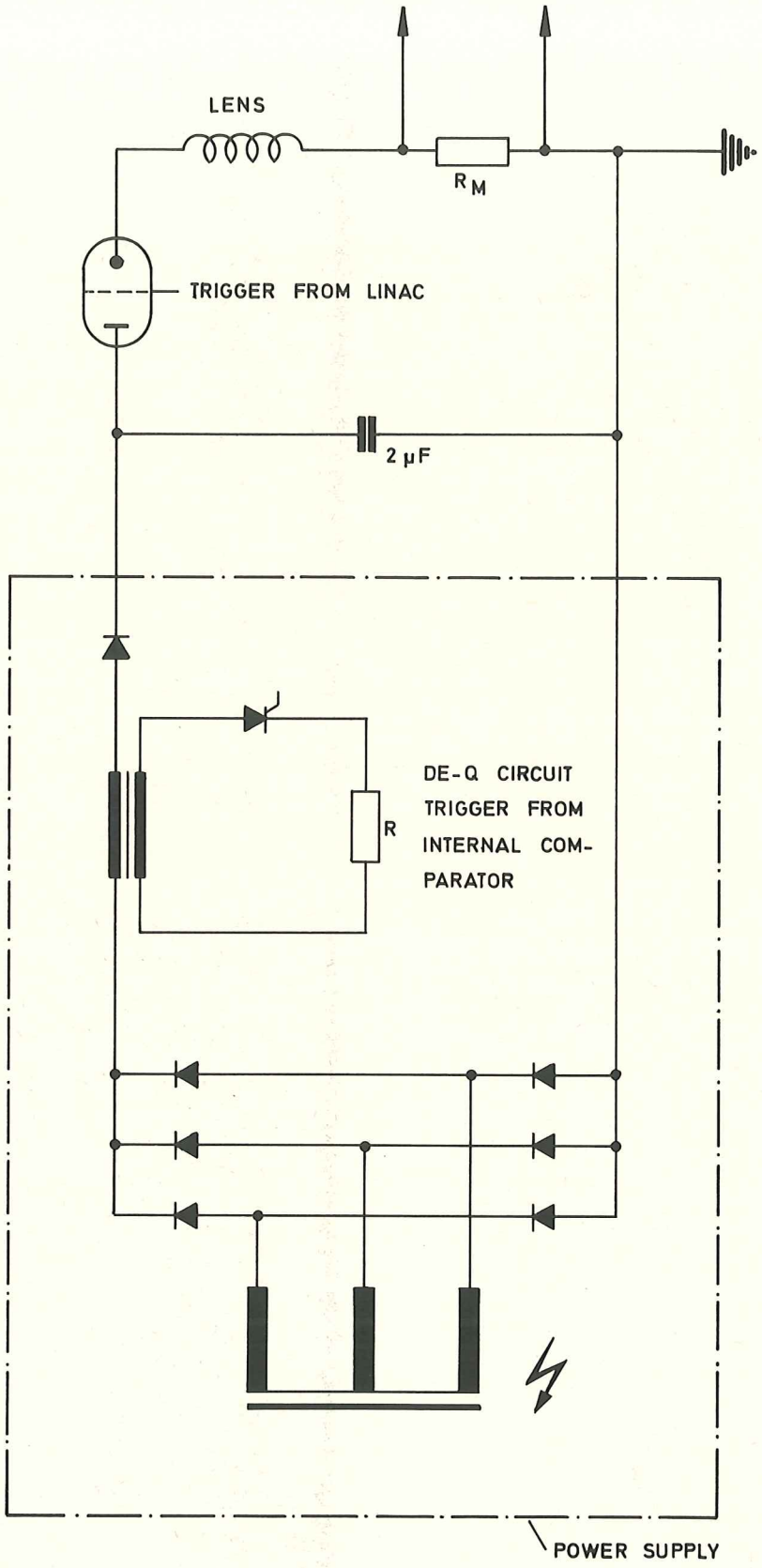

FIG. 17 ELECTRIC CIRCUIT FOR PULSE GENERATION, ROUGHLY SCHEMATIC (R_M - COAXIAL SHUNT FOR MEASURING SHORT PULSES OF HIGH CURRENT)